Available online at www.sciencedirect.com
SCIENCE DIRECT®
Acta Materialia 52 (2004) 4801–4807
Acta MATERIALIA
www.actamat-journals.com

First principles assessment of ideal fracture energies of materials with mobile impurities: implications for hydrogen embrittlement of metals

D.E. Jiang, Emily A. Carter *

Department of Chemistry and Biochemistry, University of California, 607 Charles Young Drive, P.O. Box 951569, Los Angeles, CA 90095-1569, USA

Received 20 April 2004; received in revised form 23 June 2004; accepted 23 June 2004
Available online 20 July 2004

Abstract

We propose that the ideal fracture energy of a material with mobile bulk impurities can be obtained within the framework of a Born-Haber thermodynamic cycle. We show that such a definition has the advantage of initial and final states at equilibrium, connected by well-defined and measurable energetic quantities, which can also be calculated from first principles. Using this approach, we calculate the ideal fracture energy of metals (Fe and Al) in the presence of varying amounts of hydrogen, using periodic density functional theory. We find that the metal ideal fracture energy decreases almost linearly with increasing hydrogen coverage, dropping by ~45% at one-half monolayer of hydrogen, indicating a substantial reduction of metal crystal cohesion in the presence of hydrogen atoms and providing some insight into the cohesion-reduction mechanism of hydrogen embrittlement in metals.

Keywords: Hydrogen embrittlement; Iron; Aluminum; First principles electronic structure

1. Introduction

Metals can absorb hydrogen atoms during manufacture and/or service. These dissolved hydrogen atoms can greatly affect the mechanical properties of structural metals, often leading to material failure. In particular, hydrogen frequently decreases a metal's ductility, a phenomenon given the name hydrogen embrittlement (HE). HE occurs in both polycrystalline and single crystal samples of pure metals and alloys [1–3]. Various mechanisms have been proposed to explain HE, including hydrogen-induced phase changes to form metal hydrides [4], hydrogen-enhanced localized plasticity [5–12], and cohesion reduction [13–16]. Here we focus on quantitatively assessing the latter mechanism. The idea of cohesion-reduction [17] suggests that segregation of hydrogen to an incipient fracture zone reduces the local atomic binding at the crack tip, decreasing the crystal's cohesive energy and inducing embrittlement [18]. A closely related concept is the reduced surface energy model [19,20], whereby the lowering of the surface energy by impurities increases the driving force to form two new surfaces, i.e., to form a crack.

The use of first principles techniques to investigate how impurities affect cohesive properties of materials was pioneered by Freeman and co-workers [21–23]. Their work was focused on grain boundary cohesion of iron in the presence of segregated impurities such as hydrogen, boron, carbon, nitrogen, phosphorus, or other alloying elements [24–29].

Recent work by Serebrinsky et al. [30] employs a cohesive zone mechanics model of HE, based on the cohesion-reduction mechanism. A cohesive law dependent on hydrogen concentration is required as input. Such a

* Corresponding author. Tel.: +1-310-206-5118; fax: +1-310-267-0319.
E-mail address: eac@chem.ucla.edu (E.A. Carter).

1359-6454/$30.00
doi:10.1016/j.actamat.2004.06.037

law describes the dependence of forces opposing crack formation, or tractions (force per unit area), on the incipient crack surfaces' separation distance. One key component of this law is the ideal fracture energy, i.e., the energy required to form a crack in the absence of plastic dissipative processes. The ideal fracture energy is just the cost to form the two new surfaces, which is simply twice the surface energy. In this work, we consider how to calculate the ideal fracture energy for HE from first principles, which is then used as input into higher length scale models of stress-corrosion cracking that account for plasticity at the continuum level. In order to avoid double-counting of plastic effects, in fact what we calculate here, the ideal fracture energy in the absence of plasticity, is exactly what is needed.

While it is straightforward to define an ideal fracture energy for a pure material whose composition across the sample does not change upon fracture [34,35], it is not obvious how to define an ideal fracture energy for a crystal containing mobile impurities that may move to the surface upon crack formation. Several models have been proposed to obtain the fracture energy in the presence of impurities. Fig. 1 shows two of those models, proposed by Lu et al. [31] and Van der Ven and Ceder [32]. Starting from a layer of hydrogen atoms in the bulk metal, Lu et al. simulate crystal decohesion by introducing a thick vacuum layer and letting the hydrogen atoms stay on the surface. The advantage of this model is that it is straightforward to use density functional theory (DFT) to directly calculate such a fracture energy (2γ) in one step, while the disadvantage is that the initial state is not a mechanically stable distribution of hydrogen in the bulk metal. As a result, in the high coverage regime, the initial states in this model become unstable due to the repulsion between hydrogen atoms. As we show below, such a state need not be invoked, because H in particular is a very mobile impurity, freely diffusing from one interstitial site to another.

Van der Ven and Ceder [32,33] also investigated the effects of hydrogen impurities on the decohesion of a pair of Al(1 1 1) planes by an equilibrium thermodynamic description. They determined the energy and grand force potential of the cohesive zone as a function of lattice plane separation and hydrogen coverage using both first principles DFT and a lattice gas model Hamiltonian.

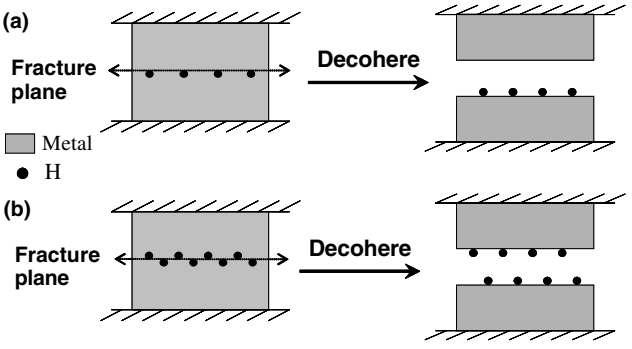

Fig. 1. Models used to calculate the fracture energy (2γ) as a function of H coverage (Θ_H) from DFT: (a) Lu et al.'s model [31]; (b) Van der Ven and Ceder's model [32,33].

In the present work, we propose a new way to obtain ideal fracture energies as a function of mobile impurity coverage from first principles. We apply this scheme to assess hydrogen-induced decohesion in Fe and Al. The rest of the paper is laid out as follows. We give calculational details in Section 2, followed by results and discussion in Section 3, and we conclude in Section 4.

2. Calculational details

We performed DFT calculations [36,37] within both the local density approximation (LDA) and the generalized gradient approximation (GGA) for electron exchange and correlation, using the Vienna Ab Initio Simulation Package [38,39]. We used both PBE [40] and RPBE [41] forms of GGA, as explained further below. We employed Blöchl's projector augmented wave (PAW) method [42], as implemented by Kresse and Joubert [43]. The PAW method is an all-electron DFT technique (within the frozen-core approximation) with the computational efficiency of pseudopotential techniques. We used the standard version of the PAW potentials for Fe, Al, and H supplied with VASP. We performed spin-polarized calculations for Fe-containing systems and non-spin-polarized calculations for Al-containing systems. We used a lattice parameter of 2.83 Å for bcc Fe, as obtained previously [44]. For fcc Al, we obtained an equilibrium lattice parameter of 4.04 Å (3.99 Å) with GGA (LDA).

We tested k-point sampling and kinetic energy cutoff convergence for all supercells. As a result of the convergence tests, we used a kinetic energy cutoff of 350 eV for all calculations, which converged total energies to 2 meV/atom. For bulk Fe supercells, we used a k-point sampling of $4\times4\times4$ and $2\times2\times2$ for Fe_{54} and Fe_{128}, respectively. For bulk Al supercells, we used a k-point sampling of $8\times8\times8$ and $6\times6\times6$ for Al_{32} and Al_{108}, respectively. The first-order Methfessel–Paxton method [45] was used for the Fermi-surface smearing in order to obtain accurate forces, and a smearing width of 0.1 eV was chosen such that the error in the extrapolated energy at 0 K is less that 1 meV/atom.

Both cell shape and atomic positions were allowed to relax for bulk calculations, while only atomic positions were allowed to change for surface calculations (the lateral cell parameters are kept to be those of the equilibrium bulk crystal). The force tolerance for structural relaxation was set to 0.01 eV/Å .

For modeling surfaces and H adsorption, we used a 10 Å thick vacuum layer and seven layers of metal atoms, with the bottom four layers fixed at their bulk positions for both Fe(1 1 0) and Al(1 1 1). These particular surfaces were examined, since they are the most stable and therefore the most likely to form upon cleavage. H was adsorbed only on one side of the slab; this produces a small dipole due to slight charge transfer from the metal to the hydrogen, however we did not bother with a dipole correction to the total energy since it was very small (<1 meV/cell). For Fe(1 1 0) supercells, we used converged k-point meshes of 14×14×1, 7×7×1, and 4×4×1 for $p(1\times1)$, $p(2\times2)$, and $p(3\times3)$ surface cells, respectively. For Al(1 1 1) supercells, we used converged k-point meshes of 16×16×1, 8×8×1, and 6×6×1 for $p(1\times1)$, $p(2\times2)$, and $p(3\times3)$ surface cells, respectively. We allowed the H layer together with the top three layers of the metal slab to relax. Residual forces on fixed atoms in the fourth metal layer are <0.01 eV/Å .

The solution enthalpies of hydrogen atoms in bulk metals and the adsorption energies of hydrogen atoms on metal surfaces are defined in the same manner:

$$\Delta E = E_{\text{H–metal}} - E_{\text{metal}} - \frac{1}{2}E_{\text{H}_2}. \quad (1)$$

Here all energies are referenced to the gaseous hydrogen molecule and the pure metal. We report in Tables 1 and 3 the ΔE on a per H atom basis. The first term on the right-hand side is the total energy of the supercell that includes n metal atoms and 1 H atom; the second term is the total energy of the supercell that consists of n metal atoms. The first two terms were calculated with the same parameters (k-point sampling, kinetic energy cut-off, etc.). The third term is half the total energy of the hydrogen molecule, which is calculated by putting H_2 in a cubic box with 10 Å sides and carrying out a Γ-point calculation. Using PBE, we obtained for H_2 an equilibrium bond length of 0.750 Å, a harmonic vibrational frequency of 4300 cm^{-1}, and a binding energy (D_e) of 4.54 eV, which are in fair agreement with experimental values of 0.741 Å, 4395 cm^{-1} and 4.75 eV [46].

For each step we consider, the zero-point energies (ZPE) for both reactants and products are estimated by summing up the zero-point vibrational energies of the normal modes of H, which can be in the metal, on the metal, or in the form of H_2. These normal modes were obtained by diagonalizing a finite difference construction of the Hessian matrix with displacements of 0.01 Å (only allowing H to move), using the PBE exchange-correlation functional. Implicit in this estimation is the assumption that the phonon spectrum of the metal does not change enough in any step to warrant its inclusion in the ZPE corrections. Given the small concentration of H and the lack of surface reconstructions in these metals, this should be a valid assumption.

3. Results and discussion

We propose here an alternative means to calculate ideal fracture energies (2γ) of materials containing mobile impurities. We illustrate the approach using hydrogen atoms as the mobile impurities. Instead of a direct fracture process as in Fig. 1, we use a Born-Haber thermodynamic cycle (Fig. 2) to compute 2γ as a function of Θ_H. We envision a scenario where a metal crystal contains mobile hydrogen atoms, which quickly segregate to the incipient crack surfaces as a crack begins to form. In this case, the initial state is always that of an equilibrium distribution of hydrogen in the bulk metal and the final state has a given coverage of hydrogen atoms on each slowly formed crack surface. We can uniquely define the ideal fracture energy then by connecting these two states via cleavage of the clean metal and the dissociative adsorption of hydrogen on the clean metal surface, as shown in Fig. 2. In particular, the Born-Haber cycle proceeds as follows. First, we remove dissolved H from the metal in step 1 (the reverse of $H_{2(g)}$ dissolution, $-\Delta H_s$), so that we can compute the well-defined cleavage energy of a pure metal crystal in step 2 [$2\gamma(0)$]. Then the hydrogen is added back via dissociative adsorption in step 3 (E_{ad}) to arrive at the final state.

Use of this thermodynamic cycle to estimate the ideal fracture energy relies on the validity of three assumptions: (i) the heat of solution of hydrogen in the bulk metal does not vary much with hydrogen concentration (see Table 1; variation of only ~0.02 eV over 0.9–3.0 and 0.78–1.8 at.% H for Al and Fe, respectively); (ii) hydrogen diffuses very fast in bulk metals (we find a barrier of H diffusion in, e.g., bcc Fe to be very small, ~0.04 eV [50]); (iii) hydrogen prefers to stay on the metal surface (we find a very small barrier (~0.02 eV [50]) for H to diffuse out to, e.g., an Fe surface and it is exothermic to do so by ~1.0 eV [50]). If these assumptions hold, then kinetics will not dominate the phenomenon and we are free to construct any thermodynamic cycle that is convenient to arrive at the ideal fracture energy. Both our

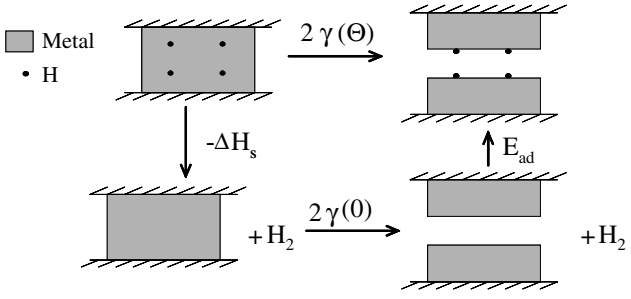

Fig. 2. The Born-Haber cycle used to calculate the ideal fracture energy [$2\gamma(\Theta_H)$] along a certain plane of a single crystal at a hydrogen atom coverage Θ_H. ΔH_s: solution enthalpy of H_2 in the bulk metal. $\gamma(0)$: surface energy of the pure metal without hydrogen. E_{ad}: dissociative adsorption energy of H_2 to form $H_{(ad)}$ on metal surfaces.

Table 1
Solution enthalpies (ΔH_s, eV/H atom) of H_2 in Al and Fe, with hydrogen atoms occupying tetrahedral sites in fcc Al and bcc Fe

Cell size	ΔH_s (eV/H)		
	LDA	GGA–PBE	Expt.
Al32	0.45	0.71 (0.73)	0.83[a], 0.66[b]
Al108	0.43	0.69 (0.71)	
Fe54	–	0.20 (0.30)	0.30[c]
Fe128	–	0.19 (0.29)	

Zero-point-energy corrected values are in parentheses.
[a] Ref. [47].
[b] Ref. [48].
[c] Ref. [49].

calculations and available experiments [49,51,52] show that these assumptions are good for hydrogen in Fe and Al.

After we obtain the energetics for each of the three steps, we use Eq. (2) to calculate the ideal fracture energy as a function of hydrogen coverage. We now discuss the three steps in detail

$$2\gamma(\Theta_H) = -\Delta H_s + 2\gamma(0) + E_{ad}(\Theta_H). \quad (2)$$

We first look at the dissolution of H_2 in a metal. Ion-channeling experiments [49] and DFT–LDA studies [31,53] confirm that hydrogen atoms prefer the tetrahedral (t) over the octahedral (o) site in fcc Al. Magnetic spin precession studies of muons suggested [54] that hydrogen atoms also prefer the t-site in bcc Fe, consistent with our recent DFT–GGA results [50]. However, DFT studies by us and others [55] show the t-site and the o-site are very close in energy and definitive experimental evidence is lacking about the site preference. Table 1 shows the H_2 solution enthalpies per H atom in Al and Fe, assuming t-site occupancy. Although the LDA describes bulk Al quite accurately, the GGA is needed to give H_2 solution enthalpies within the range measured by experiment. This is supported by a recent detailed DFT–GGA study of H in Al, which yields a H_2 solution enthalpy in Al identical to ours [56]. For Fe, it is well known that the GGA is necessary for an accurate description of its bulk properties. In the case of Fe, the solution enthalpies are in good agreement with experiment when ZPE corrections are included. H_2 dissolution is endothermic for both Al and Fe, with Al 0.40 eV more endothermic. This finding for Al agrees with earlier DFT–LDA results of de Vita and Gillan [53]. By contrast, recent DFT–LDA calculations by Lu et al. [31] proposed that the H impurity is thermodynamically stable in bulk Al, in disagreement with both experiment [47,48], earlier theory [53], and our findings here. The significant endothermicity found for dissolving hydrogen in Al is consistent with the very low measured solubilities of H in Al [57].

We now consider the second step, cleavage of the pure metal to form the most stable surfaces of each metal. We therefore examine formation of Al(1 1 1) and Fe(1 1 0), which are the closest-packed surfaces of Al and Fe. As Table 2 indicates, DFT–GGA (with the PBE exchange-correlation functional) predicts the surface energy of Fe(1 1 0) to be 2.43 J m^{-2}, in agreement with experiment [58]. DFT–GGA(PBE) yields a surface energy of Al(1 1 1) lower than experiment by ~13%. Considerable uncertainty exists in measured surface energies (usually derived from liquid contact angle measurements); the DFT–GGA(PBE) predictions for the crystal may be as reliable as the measured values for the liquid.

The third step in the Born-Haber cycle is the dissociative adsorption of hydrogen on Fe(1 1 0) and Al(1 1 1). In earlier work, we examined hydrogen adsorption on Fe(1 1 0), finding that H atoms prefer the quasi-threefold site on Fe(1 1 0) at all coverages (0.25–1.0 ML (monolayer)) [60], in agreement with experiment [61]. H atoms prefer the fcc hollow site on Al(1 1 1), as predicted in previous DFT–LDA and DFT–GGA(PBE) studies [31,62]. While the PBE [40] exchange-correlation functional often performs very well, it is known that it tends to overbind adsorbates to surfaces by ~30% compared with experiment [41]. H/Fe(1 1 0) shows this tendency, as displayed in Table 3. However, this overbinding can be corrected with the RPBE exchange-correlation functional, as demonstrated by others [41] and our own work [60]. DFT–GGA(RPBE) predicts the dissociative adsorption energy of H_2 on Fe(1 1 0) to be ~−0.52 eV/H for Θ_H ~0.11–0.50 ML, in excellent agreement with experiment (−0.525 ± 0.05 eV [51]). As the coverage decreases from 1 ML, the adsorption energy becomes more negative (larger energy release), converging at ~0.25 ML. Repulsive interactions between adsorbed hydrogen atoms at 1ML reduce the binding energy of H to the surface. The slight hydridic character of H on Fe(1 1 0) may be responsible for the lateral repulsion.

Unfortunately, no experimental thermal desorption data are available for comparison of the adsorption energies for hydrogen on Al(1 1 1), perhaps due to the tendency of atomic hydrogen to etch Al(1 1 1) upon heating [63]. Instead, alane (aluminum hydride) oligomers have been observed to form on Al(1 1 1) [64], with thermal desorption of H/Al(1 1 1) producing many gaseous Al–H species, such as AlH_3 and Al_2H_6 [65]. Moreover, first principles calculations have predicted that chemisorbed H can cause faceting of Al(1 1 1) [62]. Here we focus only on H_2 adsorption on and absorption in aluminum, and

Table 2
Surface energies of Al(1 1 1) and Fe(1 1 0)

Surface	$\gamma(0)$ (J m^{-2})		
	LDA	GGA(PBE)	Expt.
Al(1 1 1)	0.84	1.00	1.143[a], 1.160[b]
Fe(1 1 0)	–	2.43	2.41[a]

[a,b] Estimate from experimental liquid surface tension data [58,59].

Table 3
Adsorption energies (E_{ad}, eV/H atom) of H_2 on Al(1 1 1) and Fe(1 1 0), with hydrogen occupying quasi-threefold sites on Fe(1 1 0) and fcc hollow sites on Al(1 1 1)

Θ_H (ML)	E_{ad} (eV/H): Fe(1 1 0)		E_{ad} (eV/H): Al(1 1 1)		
	PBE	RPBE	LDA	PBE	RPB*E*
1.0	−0.63	−0.47 (−0.41)	0.04	0.27	0.39 (0.37)
0.5	−0.72	−0.56 (−0.52)	0.02	0.25	0.37 (0.36)
0.25	−0.72	−0.55 (−0.51)	0.00	0.23	0.35 (0.34)
0.111	−0.71	−0.55 (−0.52)	−0.02	0.23	0.34 (0.33)
Expt.	−0.525 ± 0.05[a]			–	

Zero-point-energy corrected values are in parentheses.
[a] From temperature programmed desorption for $\Theta_H = 0.22$–0.45 ML [51].

not on the desorption process. Comparing LDA, PBE, and RPBE results in Table 3, we see that PBE reduces the LDA overbinding of H–Al(1 1 1) by ~0.25 eV, while RPBE reduces the PBE result further by ~0.10 eV. If we believe that RPBE gives reasonable predictions of adsorption energies, as we found for H/Fe(1 1 0), then the adsorption of hydrogen on Al(1 1 1) starting from H_2 and pure Al(1 1 1) is significantly endothermic. Again, as the coverage decreases, the adsorption energy becomes less positive, also indicating some small repulsive interactions among hydrogen atoms on Al(1 1 1) at higher coverages.

Now that we have all the energetics needed for the Born-Haber cycle, we then use Eq. (2) to compute γ as a function of Θ_H. For ΔH_s, we use the ZPE-corrected DFT–GGA value of 0.29 eV/H and 0.71 eV/H from Table 1 for Fe and Al, respectively. For $\gamma(0)$, we use the DFT–GGA value of 2.43 J m^{-2} for Fe(1 1 0), but the average experimental value of 1.15 J m^{-2} for Al(1 1 1), since DFT–GGA may underestimate $\gamma(0)$ for Al(1 1 1) by 13%. No matter which of these values for Al is used for $\gamma(0)$, our conclusions remain unaffected. For E_{ad}, we use the ZPE-corrected DFT–GGA–RPBE values from Table 3. Note that we need to normalize ΔH_s and E_{ad} with respect to surface area in order to use Eq. (2). (Appendix A illustrates the normalization procedure.)

We show the surface-area normalized Born-Haber cycle energetics in Table 4. The surface-area normalized ΔH_s is strictly linear with Θ_H, but the surface-area normalized E_{ad} is not strictly linear with Θ_H due to the repulsion between hydrogen atoms at higher coverages. The magnitudes of the normalized ΔH_s and E_{ad} increase with Θ_H because the number of hydrogen atoms per unit area of surface increases with Θ_H.

The resulting $\gamma(\Theta_H)/\gamma(0)$ vs. Θ_H relation is displayed in Fig. 3 for the H/Fe and H/Al systems. We observe an almost linear decrease of $\gamma(\Theta_H)$ with Θ_H for both H/Fe and H/Al. At 1.0 ML, $\gamma(\Theta_H)$ is 19% and 33% of $\gamma(0)$ for H/Fe and H/Al, respectively. This dramatic decrease of fracture energy provides a driving force for HE, since the reduced surface energy (i.e., the increased stability of the surfaces) as the hydrogen coverage increases means it will be more favorable to form a crack as the local H-concentration rises.

We know from Eq. (2) that the decrease in the surface energy comes from the difference between ΔH_s and E_{ad}, i.e., the competition between the propensity for H to stay on the surface versus remaining in the bulk crystal. For both Fe and Al, hydrogen strongly prefers to stay on the surface instead of in the bulk. This preference provides a driving force to decohere metal, thereby causing embrittlement. The linear relationship between

Table 4
Surface-area normalized solution enthalpies (ΔH_s), adsorption energies (E_{ad}), and ideal fracture energies ($2\gamma(\theta)$ from Eq. (2)) as a function of hydrogen coverage, Θ_H, for H/Fe and H/Al

System	Θ_H	$-\Delta H_s$ (J m^{-2})	E_{ad} (J m^{-2})	$2\gamma(\theta)$ (J m^{-2})
H/Fe	0	0	0	4.86
	0.111	−0.18	−0.33	4.35
	0.25	−0.41	−0.72	3.73
	0.50	−0.82	−1.47	2.57
	1.00	−1.64	−2.31	0.91
H/Al	0	0	0	2.30
	0.111	−0.36	0.17	2.11
	0.250	−0.80	0.38	1.88
	0.500	−1.61	0.82	1.51
	1.00	−3.22	1.68	0.76

Zero-point-energy corrections are included for all the energetics involving H.

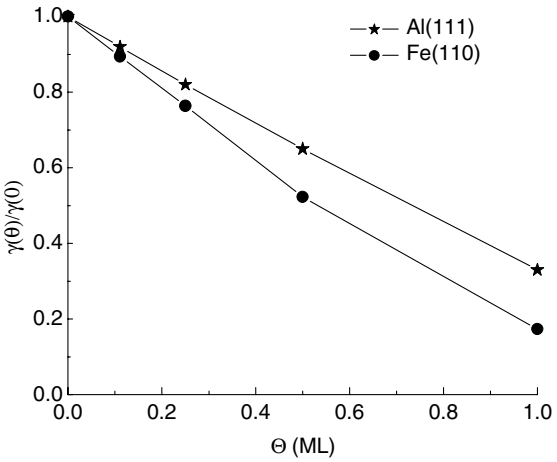

Fig. 3. Decrease in normalized surface energies $\gamma(\Theta_H)$ /$\gamma(0)$ for H-covered Al(1 1 1) and Fe(1 1 0) as hydrogen coverage (Θ_H) increases.

$\gamma(\Theta_H)/\gamma(0)$ and Θ_H results from the fact that E_{ad} does not change much with Θ_H on Fe(1 1 0) or Al(1 1 1) (see Table 3) and ΔH_s does not change much with hydrogen concentration for H in bulk Fe or Al (see Table 1). However, Table 3 reveals that E_{ad} varies less with Θ_H for H/Al(1 1 1) than for H/Fe(1 1 0), so that the normalized E_{ad} is more linear with Θ_H for H/Al(1 1 1) than for H/Fe(1 1 0), thereby producing a more linear relationship between $\gamma(\Theta_H)/\gamma(0)$ and Θ_H for Al than for Fe.

Based on these embrittlement functions, $\gamma(\Theta_H)/\gamma(0)$, one can see why steel is more readily embrittled in the presence of a hydrogen source compared to aluminum. Moreover, given the much higher endothermicity for the dissolution of hydrogen in Al compared to Fe, as well as the propensity for Al to form aluminum hydrides upon hydrogen adsorption on its surfaces, it may be that the more likely mechanism for HE in Al is not cohesion reduction at all, but rather is either hydrogen-induced localized plasticity [31,66] or perhaps even more likely, H-related phase changes to form bulk Al hydrides.

It should be noted that real fracture is very different from the ideal fracture we investigate here. Plasticity, which dominates the real fracture energy, is not included in our calculation but is taken into account in continuum level models of HE, which use the coverage-dependent ideal fracture energy from our work as input [30]. In fact, the reason that we calculate the fracture energy in the absence of plasticity is to avoid double-counting of plastic effects. Moreover, in our calculation of ideal fracture energies, we assume a slow cracking process, but crack growth rates in real fracture [1] can be higher than the diffusion rates of H in metals (this is even so for fast diffusion of H in bcc Fe and more so for the relatively slow diffusion of H in fcc Al). Thus, the kinetics of H segregation to the crack tip or the newly fractured surfaces can govern the cohesion reduction as the crack propagates, and may cause a time-delayed cracking behavior [3]. This is precisely why intermittent cracking for H in Fe is observed in continuum modeling of HE [30].

4. Conclusions

We propose that the ideal fracture energy (or surface energy) of a material with mobile impurities can be readily calculated within the framework of a Born-Haber thermodynamic cycle. We show that such a definition utilizes equilibrium states along the path, connected by well-defined and measurable energetic quantities. Here we apply this approach to calculate the ideal fracture energy of metals in the presence of hydrogen, using periodic DFT. To calculate the energy change from an equilibrium distribution of hydrogen atoms in bulk metals to fractured metal surfaces covered with hydrogen atoms, we divided the process into three steps, each of which can be straightforwardly calculated with DFT or measured independently. Here we focused on H in Fe and Al, providing some insight into the likelihood of the cohesion-reduction mechanism of HE in these metals. This model easily can be applied to study the cohesion-reduction mechanism of impurity embrittlement that may occur in other metals.

Acknowledgements

This work was supported by the Army Research Office and the DOD-MURI program. We thank the Maui High Performance Computing Center and the NAVO Major Shared Resources Center for providing CPU time. We also thank Prof. G. Ceder for useful discussions.

Appendix A. Surface area normalization of the energetics

To show how we normalize the energetics from Tables 1 and 3, we use H/Fe as an example. Suppose we start with two H atoms in an infinite bulk Fe crystal, separating to having one H atom on each incipient crack surface. We wish to normalize by the appropriate area of the cleavage plane unit cell. For $\Theta_H = 1$ ML, we consider the surface (1×1) cell, which has a surface area of 5.68 Å^2. So the normalized ΔH_s will simply be

$$\Delta H_s = 0.29\ \text{eV/H} \times 2\ \text{H}/5.68\ \text{Å}^2 = 0.102\ \text{eV Å}^{-2} = 1.64\ \text{J m}^{-2}.$$

And the normalized E_{ad} will be

$$E_{ad} = -0.41\ \text{eV/H} \times 2\ \text{H}/5.68\ \text{Å}^2 = -0.144\ \text{eV Å}^{-2} = -2.31\ \text{J m}^{-2}.$$

For $\Theta_H = 0.50$ ML, we consider the surface (2×1) cell, which has a surface area of $5.68 \times 2 = 11.36$ Å^2. In the same way, we normalize ΔH_s and E_{ad} as follows:

$$\Delta H_s = 0.29 \text{ eV/H} \times 2 \text{ H}/11.36 \text{ Å}^2 = 0.051 \text{ eV Å}^{-2} = 0.82 \text{ J m}^{-2}.$$

$$E_{ad} = -0.52 \text{ eV/H} \times 2 \text{ H}/11.36 \text{ Å}^2 = -0.092 \text{ eV Å}^{-2} = -1.47 \text{ J m}^{-2}.$$

The normalization for $\Theta_H = 0.25$ and 0.111 ML and for H/Al is carried out in precisely the same manner.

References

[1] Oriani RA, Hirth JP, Smialowski M. Hydrogen Degradation of Ferrous Alloys. Westwood (NJ): Noyes Publications; 1985.
[2] Wang J-S. Eng Fract Mech 2001;68:647.
[3] Wang J-S. Solid Mech Appl 2001;84:31.
[4] Westlake DG. Trans ASM 1969;62:1000.
[5] Beachem CD. Metall Trans 1972;3:437.
[6] Eastman J, Matsumoto T, Narita N, Heubaum F, Birnbaum HK. In: Bernstein IM, Thompson AW, editors. Hydrogen in Metals. New York: Metallurgical Society of AIME; 1981. p. 397.
[7] Tabata T, Birnbaum HK. Scr Metall 1984;18:231.
[8] Robertson IM, Birnbaum HK. Acta Metall 1986;34:353.
[9] Shih DS, Robertson IM, Birnbaum HK. Acta Metall 1988;36:111.
[10] Birnbaum HK, Sofronis P. Mater Sci Eng A 1994;176:191.
[11] Ferreira PJ, Robertson IM, Birnbaum HK. Acta Mater 1998;46:1749.
[12] Sofronis P, Robertson IM. Phil Mag A 2002;82:3405.
[13] Troiano AR. Trans ASM 1960;52:54.
[14] Oriani RA. Ber Bunsenges Phys Chem 1972;76:848.
[15] Oriani RA, Josephic PH. Acta Metall 1977;25:979.
[16] Oriani RA. Ann Rev Mater Sci 1978;8:327.
[17] Rice JR, Wang JS. Mater Sci Eng 1989;A107:23.
[18] Vehoff H, Klameth HK. Acta Metall 1985;33:955.
[19] Petch NJ. Phil Mag 1956;1:331.
[20] Tromans D. Acta Metall Mater 1994;42:2043.
[21] Wu R, Freeman AJ, Olson GB. J Mater Res 1992;7:2403.
[22] Wu R, Freeman AJ, Olson GB. Phys Rev B 1993;47:6855.
[23] Wu R, Freeman AJ, Olson GB. Science (Washington, DC) 1994;265:376.
[24] Wu R, Freeman AJ, Olson GB. Phys Rev B 1996;53:7504.
[25] Geng WT, Freeman AJ, Wu R, Geller CB, Raynolds JE. Phys Rev B 1999;60:7149.
[26] Zhong L, Wu R, Freeman AJ, Olson GB. Phys Rev B 2000;62:13938.
[27] Geng WT, Freeman AJ, Wu R, Olson GB. Phys Rev B 2000;62:6208.
[28] Geng WT, Freeman AJ, Olson GB. Phys Rev B 2001;63:165415/1.
[29] Kim M, Geller CB, Freeman AJ. Scr Mater 2004;50:1341.
[30] Serebrinsky S, Carter EA, Ortiz M. J Mech Phys Solids 2004 (in press).
[31] Lu G, Orlikowski D, Park I, Politano O, Kaxiras E. Phys Rev B 2002;65.
[32] Van der Ven A, Ceder G. Phys Rev B 2003:67.
[33] Van der Ven A, Ceder G. Acta Mater 2004;52:1223.
[34] Jarvis EAA, Hayes RL, Carter EA. Chem Phys Chem 2001;2:55.
[35] Hayes RL, Ortiz M, Carter EA. Phys Rev B 2004;69:172104.
[36] Hohenberg P, Kohn W. Phys Rev B 1964;136:864.
[37] Kohn W, Sham LJ. Phys Rev A 1965;140:1133.
[38] Kresse G, Furthmüller J. Phys Rev B 1996;54:11169.
[39] Kresse G, Furthmüller J. Comp Mater Sci 1996;6:15.
[40] Perdew JP, Burke K, Ernzerhof M. Phys Rev Lett 1996;77:3865.
[41] Hammer B, Hansen LB, Nørskov JK. Phys Rev B 1999;59:7413.
[42] Blöchl PE. Phys Rev B 1994;50:17953.
[43] Kresse G, Joubert D. Phys Rev B 1999;59:1758.
[44] Jiang DE, Carter EA. Phys Rev B 2003;67:214103.
[45] Methfessel M, Paxton AT. Phys Rev B 1989;40:3616.
[46] Huber KP, Herzberg G. Molecular Spectra and Molecular Structure, 4: Constants of Diatomic Molecules. New York: Van Norstrand Reinhold Co.; 1979.
[47] Ransley CE, Neufeld H. J Inst Met 1948;74:599.
[48] von Eichenauer W. Z Metallkd 1968;59:613.
[49] Hirth JP. Metal Trans A 1980;11A:861.
[50] Jiang DE, Carter EA. Phys Rev B 2004 (in press).
[51] Kurz EA, Hudson JB. Surf Sci 1988;195:15.
[52] Young GA, Scully JR. Acta Mater 1998;46:6337.
[53] de Vita A, Gillan MJ. J Phys Condens: Matter 1992;4:599.
[54] Seeger A. Phys Lett A 1976;58A:137.
[55] Miwa K, Fukumoto A. Phys Rev B 2002;65:155114.
[56] Wolverton C, Ozolins V, Asta M. Phys Rev B 2004;69:144109.
[57] Massalski TB. Binary Alloy Phase Diagrams. 2nd ed. Materials Park, OH: ASM International; 1990.
[58] Tyson WR, Miller WA. Surf Sci 1977;62:267.
[59] de Boer FR, Boom R, Mattens WCM, Miedema AR, Niessen AK. Cohesion in Metals. Amsterdam: North-Holland; 1988.
[60] Jiang DE, Carter EA. Surf Sci 2003;547:85.
[61] Hammer L, Landskron H, Nichtl-Pecher W, Fricke A, Heinz K, Müller K. Phys Rev B 1993;47:15969.
[62] Stumpf R. Phys Rev Lett 1997;78:4454.
[63] Crane EL, Nuzzo RG. J Phys Chem B 2001;105:3052.
[64] Go EP, Thuermer K, Reutt-Robey JE. Surf Sci 1999;437:377.
[65] Hara M, Domen K, Onishi T, Nozoye H. J Phys Chem 1991;95:6.
[66] Lu G, Zhang Q, Kioussis N, Kaxiras E. Phys Rev Lett 2001;87:095501.